Strain-induced quantum topological phase transitions in Na_{3}Bi

Dexi Shao, Jiawei Ruan, Juefei Wu, Tong Chen, Zhaopeng Guo, Haijun Zhang, Jian Sun, Li Sheng, and Dingyu Xing

Phys. Rev. B **96**, 075112 — Published 8 August 2017

DOI: 10.1103/PhysRevB.96.075112

Strain-induced quantum topological phase transitions in Na_3Bi

Dexi Shao[1], Jiawei Ruan[1], Juefei Wu[1], Tong Chen[1], Zhaopeng Guo[1],
Haijun Zhang[1,2], Jian Sun[1,2],* Li Sheng[1,2], and Dingyu Xing[1,2]
[1] *National Laboratory of Solid State Microstructures and Department of Physics, Nanjing University, Nanjing 210093, China*
[2] *Collaborative Innovation Center of Advanced Microstructures, Nanjing 210093, China*

Strain can be used as an effective tool to tune the crystal structure of materials and hence to modify their electronic structures, including topological properties. Here, taking Na_3Bi as a paradigmatic example, we demonstrated with first-principles calculations and $\mathbf{k}\cdot\mathbf{p}$ models that the topological phase transitions can be induced by various types of strains. For instance, the Dirac semimetal phase of ambient Na_3Bi can be tuned into a topological insulator (TI) phase by uniaxial strain along the $\langle 100\rangle$ axis. Hydrostatic pressure can let the ambient structure transfer into a new thermodynamically stable phase with $Fm\bar{3}m$ symmetry, coming with a perfect parabolic semimetal having a single contact point between the conduction and valence bands, exactly at Γ point on the Fermi level like $\alpha-Sn$. Furthermore, uniaxial strain in the $\langle 100\rangle$ direction can tune the new parabolic semimetal phase into a DSM, while shear strains in both the $\langle 100\rangle$ and $\langle 111\rangle$ directions can take the new parabolic semimetal phase into a TI. $\mathbf{k}\cdot\mathbf{p}$ models are constructed to gain more insights into these quantum topological phase transitions. At last, we calculated surface states of $Fm\bar{3}m$ Na_3Bi without and with strains to verify these topological transitions.

I. INTRODUCTION

Due to the inspiration from fundamental physics and interest in exotic properties for applications, new topological materials and phases with non-trivial band topology, such as topological insulators (TIs), topological metals/semimetals and topological superconductors, attracted tremendous attention in the past decade. [1–4] The non-trivial states are usually protected by certain symmetries, such as time-reversal symmetry (TRS), crystalline symmetry including inversion symmetry (IS). Among these topological states, TRS-protected surface states were first predicted in 1987[5] to occur in quantum wells of HgTe sandwiched between CdTe and were successfully observed in experiments in 2006[6]. In 3D TIs , the surface state is actually a new type of two-dimensional (2D) massless electron gas, with its spin locked to its momentum [7,8]. These robust metallic surface states differ TIs from normal insulators and make TIs greatly attractive.

Compared with TIs indexed by Z_2, topological semimetals, in which band crossings appear at Fermi level in a reduced dimension, have attracted more attention because they may supply platforms to investigate new types of fermion-like excitations, including Dirac fermions[9,10], Weyl fermions[11–14] and nodal lines[15–20], etc. Among them, the earliest example may be the 2D Dirac semimetal – graphene[21,22]. Interestingly, later works show that the surface states in 3D TIs also present 2D massless Dirac-like dispersions. Among many candidates with Dirac-like dispersions have been reported[9,10,23,24], Cd_3As_2 and Na_3Bi are particularly attractive 3D Dirac semimetals with their Dirac points locating exactly at the Fermi level. Featured by 3D Dirac points in the bulk and Fermi arcs on the surface[9,10,23,25], 3D Dirac semimetals have recently been identified experimentally in Cd_3As_2[26–30] and Na_3Bi systems[31,32].

Na_3Bi was predicted to be a 3D bulk Dirac semimetal[9] and verified later by experiments[31]. This topological Dirac fermion in Na_3Bi is protected by TRS and IS together with R_{3z} symmetry. It is known that breaking of the R_{3z} symmetry, for example 1% compression along the y axis, will change the system into a TI with $Z_2 = 1$[1,2]. After the predictions of Na_3Bi to be a 3D Dirac semimetal, large efforts were invested to study this interesting system, for instance, Fermi arc surface states[32], quantum oscillations[33], evidence for the chiral anomaly[34], magnetoresistance[35], etc. As we know, alkali pnictides A_3B (A = alkali metal, B = pnictide) usually crystalline into two different structures at ambient pressure: the hexagonal $P6_3/mmc$ phase (e.g., K_3Bi and Rb_3Bi) and the cubic $Fm\bar{3}m$ phase (e.g., Li_3Bi and Cs_3Bi)[36]. Actually, phonon spectra of $P6_3/mmc$ phase of Na_3Bi show negative frequencies, which means this phase should not be dynamically stable, Cheng et al.[37] reported that the ground state of Na_3Bi at ambient pressure could be a $P\bar{3}c1$ (or so-called hP24) phase, which is a distorted superlattice version of the $P6_3/mmc$ phase. And this $P\bar{3}c1$ phase also exhibits features of 3D Dirac semimetal.

Pressure and strain have been used as effective methods to modify the topological properties of materials, for instance, in graphene[38], BiTeI[39], HgTe-class[40], Cd_3As_2[41–43], TaAs[44], $ZrTe_5$[45], WTe_2[46], SnTe[47], TaP[48], etc. The work by Cheng et al.[49,50] showed that Na_3Bi would undergo a pressure-induced structural phase transition from the $P\bar{3}c1$ (hP24) phase to a cubic $Fm\bar{3}m$ (cF16) phase at pressure of about 0.8 GPa, which is in good agreement with previous experimental findings[36,51,52]. The transition pressure for Na_3Bi is such low, which means compressive strain has a large effect on the structure of this system. Previous work[50] reported that shear strain along $\langle 100\rangle$ axis can develop the cubic phase of Na_3Bi into a TI. However, whether or how different type of strain will affect the topological properties of Na_3Bi and detailed analysis with model Hamiltonian

still remains an open question.

In this work, we have studied effects of several different strains on Na_3Bi, including uniaxial tensile/compressive strain and shear strain in different directions. We find that uniaxial strain on Na_3Bi in the space group of $P\bar{3}c1$ at ambient pressure can induce a topological phase transition from Dirac semimetal to TI. With the help of Luttinger Hamiltonian[53], we also find the $Fm\bar{3}m$ phase to be a perfect parabolic semimetal. We then impose a uniaxial strain on the $Fm\bar{3}m$ lattice and find it will open a gap at the Γ point and induce a Dirac crossing near the Γ. Furthermore, with the help of a $\mathbf{k}\cdot\mathbf{p}$ model, we confirm that the term of $g\Gamma^5$ in the Hamiltonian generated from the crystal-field splitting induces the gap and the Dirac crossing in the uniaxial strained structure.

On the other hand, shear strain in the $\langle 100\rangle$ and $\langle 111\rangle$ directions can tune the $Fm\bar{3}m$ phase into a TI. To get more insights of these topological phase transitions, we develop two $\mathbf{k}\cdot\mathbf{p}$ models corresponding to the two different shear strains, respectively, and find that spin-orbit coupling (SOC) together with the splitting of the crystal field plays a key role in these transitions.

II. METHODOLOGY AND THE DETAIL

Ab initio random structure searching[54,55] is applied for crystal structure searching under pressure. Structure optimization is performed using projector augmented wave (PAW) potential[56] with the Perdew-Burke-Erzernhof[57] generalized gradient approximation (PBE-GGA) exchange-correlation functional implemented in the Vienna *ab initio* simulation package (VASP)[58] in the framework of density functional theory (DFT). The plane wave cutoff is set to 850 eV, structure relaxation is carried out until all of the atomic forces on each ion is less than 0.0025 eV/$\mathring{A}$. Electronic band structures calculations are carried out using full-potential linearized augmented plane-wave method implemented in the WIEN2k[59] package. SOC is taken into account self-consistently. $21\times21\times21$ k-mesh is used as the period boundary condition for electronic structure calculation under ambient and high pressure.

III. THE ELECTRONIC STRUCTURES OF $P\bar{3}C1$ PHASE UNDER UNIAXIAL STRAIN

A recent work reveals that the zero-pressure ground state of Na_3Bi should be the $P\bar{3}c1$ phase which presents the features of Dirac semimetal[37]. The crystal structures of the $P\bar{3}c1$ phase are shown in Fig. 1, and the corresponding lattice parameters are showed in Table. I.

There are 24 atoms in one unit cell of the $P\bar{3}c1$ phase which occupy 4 nonequivalent positions. We sign the atoms locate at these nonequivalent positions with Na1, Na2, Na3 and Bi, respectively, as shown in Fig. 1 (a). The band structure with SOC for the $P\bar{3}c1$ phase Na_3Bi is shown in Fig. 2(b), the result is similar to earlier work by Cheng et al.[37] We impose a uniaxial tensile strain along the x axis and meanwhile a compressed strain along the y axis to keep the volume unchanged. As shown in Fig. 2(a), this operation or vice versa, breaks the R_{3z} symmetry in the $P\bar{3}c1$ phase and changes the space group of the structure from $P\bar{3}c1$ to $P\bar{1}$. We take 2% uniaxial strain as an example here, and the resulting band structure with SOC is shown in Fig. 2(c). From the band structure we can assert that it is an insulator directly. Using the method by Fu and Kane[60], we can easily calculate the Z_2 index by multiplying all the parities for all the occupied bands at all time-reversal-invariant momenta (TRIMs). The results are shown in Table. II, which indicates $Z_2 = (1, 111)$ for this system. This shows that uniaxial strain will induce a topological phase transition from Dirac semimetal to TI in the $P\bar{3}c1$ phase.

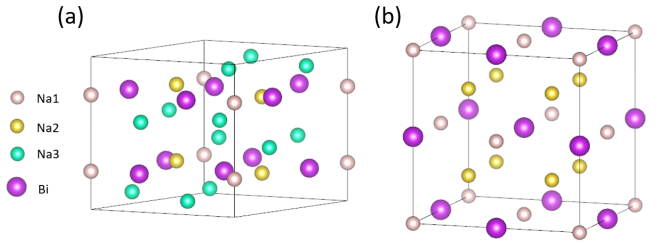

FIG. 1. (a) Crystal structure of Na_3Bi at the ambient pressure with $P\bar{3}c1$ symmetry. Na1, Na2 and Na3 atoms occupy the 2a(0,0,$\frac{1}{4}$), 4d($\frac{1}{3}$,$\frac{2}{3}$,0.200) and 12g(0.354,0.319,0.083) sites, respectively, while Bi atoms lie at the 6f(0.337,0,$\frac{1}{4}$) site. (b) Crystal structure of Na_3Bi at 1 GPa with $Fm\bar{3}m$ symmetry. Na1 and Na2 atoms occupy the 4a(0,0,0), 8c($\frac{3}{4}$,$\frac{1}{4}$,$\frac{1}{4}$) sites while Bi atoms stay at the 4b(0,0,$\frac{1}{2}$) site.

TABLE I. Lattice parameters of Na_3Bi at the ambient pressure with $P\bar{3}c1$ symmetry and 1 GPa with $Fm\bar{3}m$ symmetry.

phase	**pressure** (GPa)	$a=b$ ($\mathring{A}$)	c ($\mathring{A}$)	$\alpha=\beta$ (°)	γ (°)
$P\bar{3}c1$	0	9.459	9.674	90	120
$Fm\bar{3}m$	1	7.458	7.458	90	90

TABLE II. The product of the parities for all the occupied bands at the eight TRIMs for the $P\bar{3}c1$ phase of Na_3Bi with uniaxial strain.

TRIM	Γ	3M	3L	A	total
Parity	+	−	−	−	−

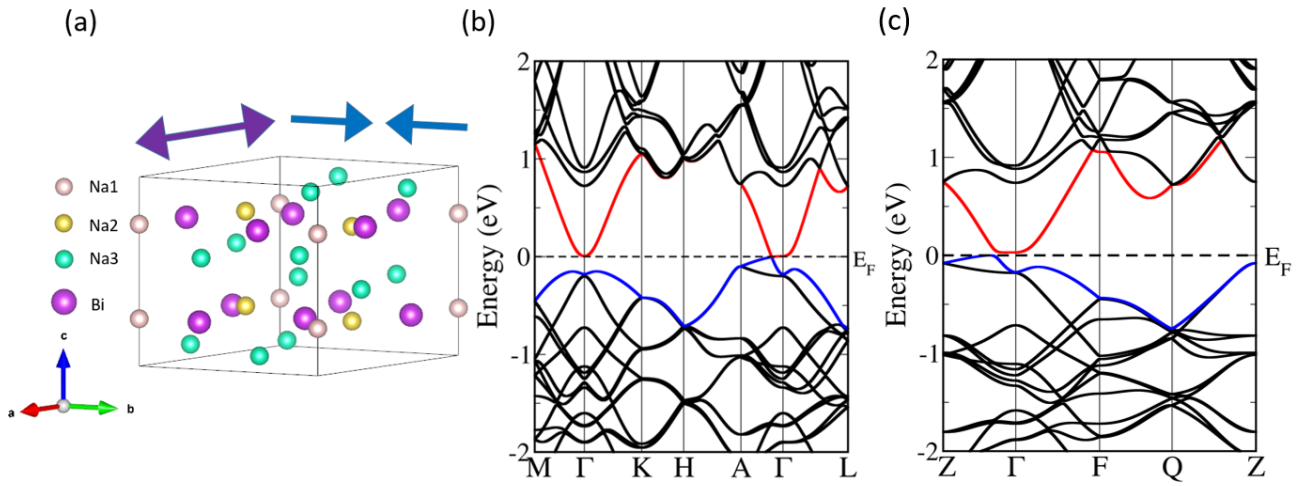

FIG. 2. (a) Crystal structure of Na_3Bi with $P\bar{3}c1$ symmetry under uniaxial strain. The purple bidirectional arrow represents tensile strain along x axis, while the two blue arrows represents compressed strain along y axis. (b) Corresponding band structure of Na_3Bi without strain and with SOC. The red and blue lines correspond to the conduction band minimum (CBM) and the valence band maximum (VBM), respectively. (c) Corresponding band structure of Na_3Bi under uniaxial strain and with SOC. The red and blue lines correspond to CBM and VBM, respectively.

IV. THE ELECTRONIC STRUCTURES OF THE HIGH-PRESSURE FM$\bar{3}$M PHASE

Crystal structure searches and thermodynamic calculations afterwards show that a cubic phase in the space group of Fm$\bar{3}$m becomes more stable than the ambient P$\bar{3}$c1 phase under the critical pressure around 0.8 GPa[50].

For the Fm$\bar{3}$m phase, there are 4 atoms occupying 3 nonequivalent positions in one primitive cell as shown in Fig. 1(b). The 4 atoms can be signed as Na1, Na1′, Na2 and Bi. Among them, Na1 and Na1′ are equivalent as a result of IS.

The detailed structural parameters of the Fm$\bar{3}$m phase are listed in Table. I. And its electronic band structures without and with SOC are illustrated in Fig. 3(a) and Fig. 3(b), similar to the results by by Cheng et al.[49]

The most interesting feature one can find in the band structures with and without SOC, as shown in Fig. 3 (a) and (b), is that there is only one touching point between the valence and conduction bands, which exactly locates at Γ point on the Fermi level. Detailed first-principle calculations without SOC indicates that this touching point is a triply degenerate point contributed most by Bi-6p$_{x,y,z}$ orbits, and the wave functions of low-energy states around the touching point mainly consist of Na-3s and Bi-6p$_{x,y,z}$ orbits. Due the fact that there are two Na1 atoms (signed with Na1 and Na1′), which are centrosymmetric connected to each other, thus we can construct bonding and antibonding states with definite parity from the s orbitals of Na1 and Na1′ atoms as follows:

$$|\mathrm{Na1}^{\pm}, s>=\frac{1}{\sqrt{2}}(|\mathrm{Na1}; s> \pm|\mathrm{Na1}'; s>) \qquad (1)$$

While there is only one atom for Na2 and Bi in the primtive cell, therefore, the parity of the orbits of Na2 and Bi atoms are only determined by their orbital angular quantum number themselves.

Taking SOC into consideration, spin and orbital angular momentum are coupled together, which generates a group of new eigenstates with certain total angular quamtum numbers. We mark these new eigenstates as $|S^{\pm}_{\mathrm{Na1},\frac{1}{2}},\pm\frac{1}{2}>$, $|S^{+}_{\mathrm{Na2},\frac{1}{2}},\pm\frac{1}{2}>$,$|S^{+}_{\mathrm{Bi},\frac{1}{2}},\pm\frac{1}{2}>$, $|P^{-}_{\mathrm{Bi},\frac{3}{2}},\pm\frac{3}{2}>$,$|P^{-}_{\mathrm{Bi},\frac{3}{2}},\pm\frac{1}{2}>$ and $|P^{-}_{\mathrm{Bi},\frac{1}{2}},\pm\frac{1}{2}>$. Here S and P denote corresponding orbits consisting of the new eigenstates and the superscripts $\pm$ represent the parities of corresponding eigenstates.

According to the analysis of irreducible representations and projected orbits, the touching point of the top of valence bands and the bottom of conduction bands (denoted as Γ_8^-) is mainly composed of $|P^{-}_{\mathrm{Bi},\frac{3}{2}},\pm\frac{3}{2}>$ and $|P^{-}_{\mathrm{Bi},\frac{3}{2}},\pm\frac{1}{2}>$ basis. We simplify the notation of these four basis as $|J, j_z>$ with $J=\frac{3}{2}$ and $j_z=\pm\frac{3}{2},\pm\frac{1}{2}$. Take the time-reversal and O_h point-group symmetries into consideration, a 4×4 Luttinger Hamiltonian[53] can exactly describe the Γ_8^- bands around the Γ point if we arrange the 4 basis in the order of $|\frac{3}{2},\frac{3}{2}>$,$|\frac{3}{2},\frac{1}{2}>$, $|\frac{3}{2},-\frac{1}{2}>$,$|\frac{3}{2},-\frac{3}{2}>$, with the Hamiltonian given by

$$H_{\mathrm{Luttinger}}(\vec{k})=\alpha_0\vec{k}^2I+\alpha_1(\vec{k}\cdot\vec{J})^2+\alpha_2\sum_{i=1}^{3}k_i^2J_i^2, \qquad (2)$$

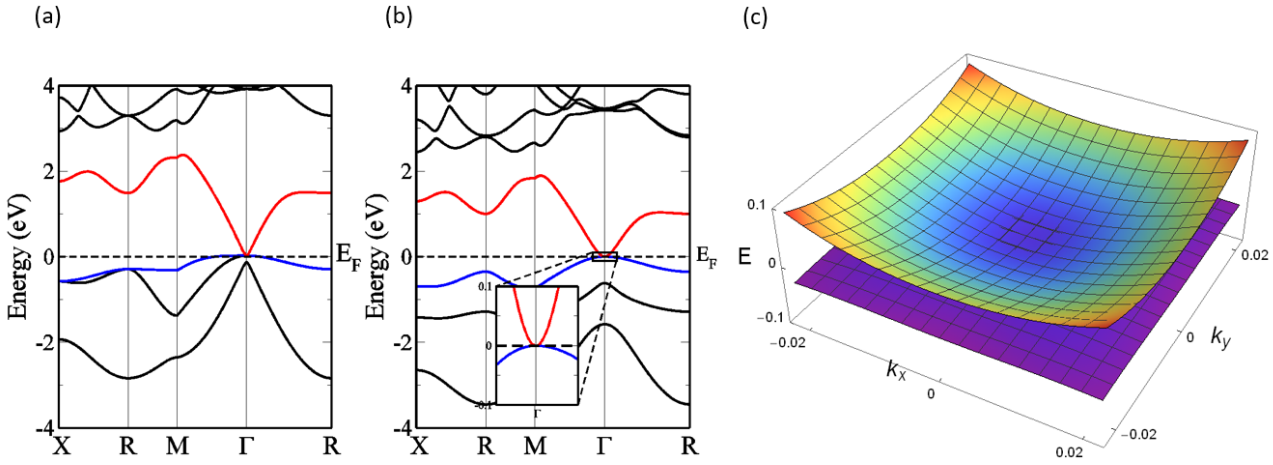

FIG. 3. The band structure of Fm$\bar{3}$m Na_3Bi (a) without soc (b) with soc at 1GPa. The red and blue lines correspond to CBM and VBM, respectively. (c) The 2D projected band structure of Fm$\bar{3}$m Na_3Bi at 1GPa in the plane of kz=0.

where $J_i (i = 1, 2, 3)$ are spin-$\frac{3}{2}$ matrices and $\alpha_i (i = 0, 1, 2)$ are parameters characterizing the band structures. These three parameters are determined as $\alpha_0 \approx 205.3\mathring{A}^2$eV,$\alpha_1 \approx -83.1\mathring{A}^2$eV,$\alpha_2 \approx -22.5\mathring{A}^2$eV by fitting the first-principle band structures around the Γ point. With this Luttinger Hamiltonian, we can nicely describe the unique parabolic dispersion near Γ at the Fermi level as shown in Fig. 3(c), which is quite different from the linear Dirac dispersions.

V. THE EFFECT OF DIFFERENT STRAIN ON THE HIGH-PRESSURE FM$\bar{3}$M PHASE

A. UNIAXIAL STRAIN ON the Fm$\bar{3}$m PHASE

When we impose a uniaxial strain ϵ along any orthogonal axis on the original Fm$\bar{3}$m structure, it will change the symmetry of the crystal from space group Fm$\bar{3}$m to I4/mmm. Here, to keep the volume of the cell invariable, when a tensile strain ϵ is applied along the z axis, we add at the same time a compressive strain $\frac{1}{\sqrt{1+\epsilon}}$ along the x and y axes, respectively. It is obvious that this operation changes the symmetry of the structure from Fm$\bar{3}$m to I4/mmm as well. The uniaxial compressive or tensile strain energy relative to the perfect Fm$\bar{3}$m structure is shown in Fig. 4 (a), which indicates that the tensile strain somehow is easier to obtain than the compressive one in this system.

With this uniaxial strain operation, as shown in Fig. 6 (a), we can predict that the triply degenerate $p_{x,y,z}$ orbits without SOC at Γ point will split into a non-degenerated p_z and a doubly degenerated $p_{x,y}$ orbits due to the crystal-field splitting.

When SOC is considered, this uniaxial strain may lead to the appearance of a Dirac crossing near the Γ point.

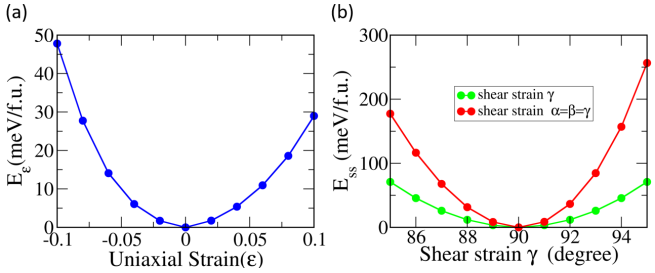

FIG. 4. Strain energy of the Fm$\bar{3}$m Na_3Bi under (a) uniaxial strain with ϵ varying from -0.1 (compressive) to 0.1 (tensile). Shear strain energy (b) along ⟨100⟩ (green) and ⟨111⟩ (red) axes with the angular parameter γ or $\alpha = \beta = \gamma$ ranging from 85° to 95°, respectively.

In fact, the uniaxial strain changes the point group of the system from O_h to D_{4h}, which also affects the $\mathbf{k} \cdot \mathbf{p}$ Hamiltonian dramatically. As the permutation symmetry of x, y, z directions is no longer preserved, J_x, J_y, J_z is not convenient to be used as basis any more. Here we use the following Γ matrices:

$$\Gamma^1 = \frac{1}{\sqrt{3}}\{J_y, J_z\}, \Gamma^2 = \frac{1}{\sqrt{3}}\{J_z, J_x\}, \Gamma^3 = \frac{1}{\sqrt{3}}\{J_x, J_y\}$$
$$\Gamma^4 = \frac{1}{\sqrt{3}}(J_x^2 - J_y^2), \Gamma^5 = J_z^2 - \frac{5}{4}, \tag{3}$$

while the other ten Γ matrices are given by $\Gamma_{ab} = \frac{1}{2i}[\Gamma_a, \Gamma_b]$. The coexistence of TRS and IS constrains that no Γ_{ab} terms exist in the model Hamiltonian. After a careful analysis of the symmetry and a tedious derivation, we can give the character table of the Γ matrices and the polynomials of momentum $\vec{k}$ as shown in Table. III using the same basis functions above-mentioned.

TABLE III. The character table for the Fm$\bar{3}$m phase of Na_3Bi under uniaxial strain along z axis.

Γ	Representation	T	$\vec{k}$
$\Gamma_0 = I$	$\tilde{\Gamma}_1^+$	+	$1, k_x^2+k_y^2, k_z^2$
$\{\Gamma_1, \Gamma_2\}$	$\tilde{\Gamma}_5^+$	+	$\{k_x k_z, k_y k_z\}$
Γ_3	$\tilde{\Gamma}_4^+$	+	$k_x k_y$
Γ_4	$\tilde{\Gamma}_3^+$	+	$1, k_x^2+k_y^2, k_z^2$
Γ_5	$\tilde{\Gamma}_1^+$	+	$k_x^2 - k_y^2$

TABLE IV. The product of the parities for all the occupied bands at the eight TRIMs for the Fm$\bar{3}$m phase of Na_3Bi under uniaxial strain along z axis.

TRIM	Γ	4N	2X	M ;	total
Parity	−	+	+	+ ;	−

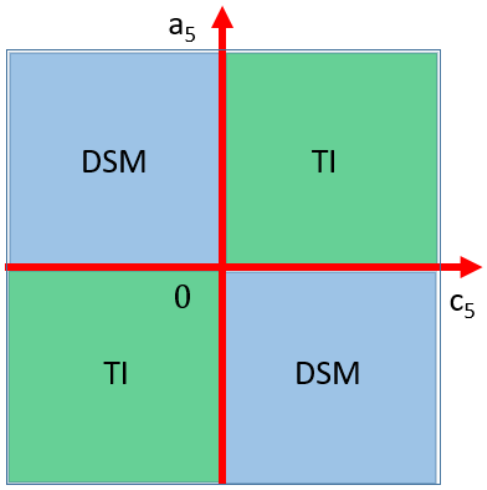

FIG. 5. Phase diagram of Fm$\bar{3}$m Na_3Bi under uniaxial strain and shear strain along the ⟨111⟩ direction from model Hamiltonian analysis using Equation (4) and (6), respectively.

Finally, from Table. III, our model Hamiltonian yields as

$$\begin{aligned} H = \sum_{i=0}^{5} f_i(\vec{k})\Gamma_i = [a_0 + b_0(k_x^2+k_y^2) + c_0 k_z^2]\Gamma_0 \\ + a_{12}(k_y k_z \Gamma_1 + k_x k_z \Gamma_2) + a_3 k_x k_y \Gamma_3 \\ + a_4(k_x^2 - k_y^2)\Gamma_4 + [a_5 + b_5(k_x^2+k_y^2) + c_5 k_z^2]\Gamma_5. \end{aligned} \quad (4)$$

The dispersion of above-mentioned model is $E(\vec{k}) = f_0(\vec{k}) \pm \sqrt{f_1^2(\vec{k}) + f_2^2(\vec{k}) + f_3^2(\vec{k}) + f_4^2(\vec{k}) + f_5^2(\vec{k})}$ and both dispersions are doubly degenerated. As a result, a band crossing of this model requires $f_1 = f_2 = f_3 = f_4 = f_5 = 0$, i.e. $k_z \neq 0 \cap k_x = k_y = 0 \cap a_5 c_5 < 0$. It means that we can always find a Dirac crossing along k_z direction when $a_5 c_5 < 0$ stands, and the location of the crossing is $\vec{k} = (0, 0, \pm\sqrt{-\frac{a_5}{c_5}})$. Otherwise, a gap near the Γ point induced by $a_5\Gamma_5$ will always preserve.

When the bands are gapped, the existence of both the TRS and IS in the uniaxial-strained Fm$\bar{3}$m Na_3Bi enables us to calculate Z_2 using Fu and Kane's method[60]. The results are listed in Table. IV, which indicates $Z_2 = (1, 000)$.

Note that the Z_2 index remains unchanged when we tune any parameters in the above-mentioned model because band inversion between $|\frac{3}{2}, \pm\frac{3}{2}>$ and $|\frac{3}{2}, \pm\frac{1}{2}>$ can not bring the parity inversion (the parities of both the two doublets at Γ are -1). So we can give resulting phase diagram of Fm$\bar{3}$m Na_3Bi under uniaxial strain shown in Fig. 5. Which shows that, the system belongs to TI when $a_5 c_5 > 0$, while it transforms into DSM in case of $a_5 c_5 < 0$.

First-principles calculations indicates the Dirac crossing always exists under a strain ϵ ranging from -10% to 10%. Which means $a_5 c_5 < 0$ always stands for uniaxial-strained structure under strains within this range.

We have chosen a uniaxial strain of $\epsilon = -4\%$ onto the Fm$\bar{3}$m phase to verify our predictions, the corresponding band structures without and with SOC are showed in Fig. 6 (b) and (c) respectively. As showed in Fig. 6(c), the appearance of this Dirac dispersion is very similar to HgTe-class materials[40], which can also be described with an additional Γ_5 term in the Luttinger Hamiltonian [53]. The difference is, in HgTe-class, with tensile stain along the z axis, the energy of p_z becomes smaller than $p_{x,y}$, while with compressive strain along the z axis, the energy of p_z becomes larger than $p_{x,y}$ when SOC is ignored. But in Na_3Bi, as shown in Fig. 6(d), both tensile and compressive stain leads to the same result that $E_{p_{x,y}}$ is always larger than E_{p_z}.

Here we give a qualitative explanation. Uniaxial strain along the z axis generates a perturbation $\mathcal{H}_{\text{strain:Na1;Na2}} = -g_{1,2}(J_z^2 - \frac{5}{4})$. Here $\mathcal{H}_{\text{strain:Na1;Na2}}$ denotes the crystal perturbation on $|\text{Bi}, p>$ from the effect of the strain on Na1 and Na2, respectively. From the unstrained structure in Fig. 6(a), we find that six Na1 atoms around the body-centered Bi atom form an octahedron while eight Na2 atoms form a cubic. We further consider the effect of the Na1-octahedron and Na2-cubic on $|\text{Bi}, p>$ by removing all the Na2 or Na1 atoms, respectively. As the blue and the green lines shown in Fig. 6(d), first-principle calculations of these two different cases indicate that with the absence of Na2-cubic, $g_1 < 0$ ($g_1 > 0$) corresponds to the tensile strain (the compressive strain); while we remove Na2 cubic, $g_2 > 0$ ($g_2 < 0$) corresponds the tensile strain (the compressive strain). However, $g_1 + g_2$ is always less than 0 for both tensile and compressive strain, which means Na1-octahedron effects $Bi, p_{x,y}$ more in the tensile strain case, while Na2-cubic effects more in the compressed strain case.

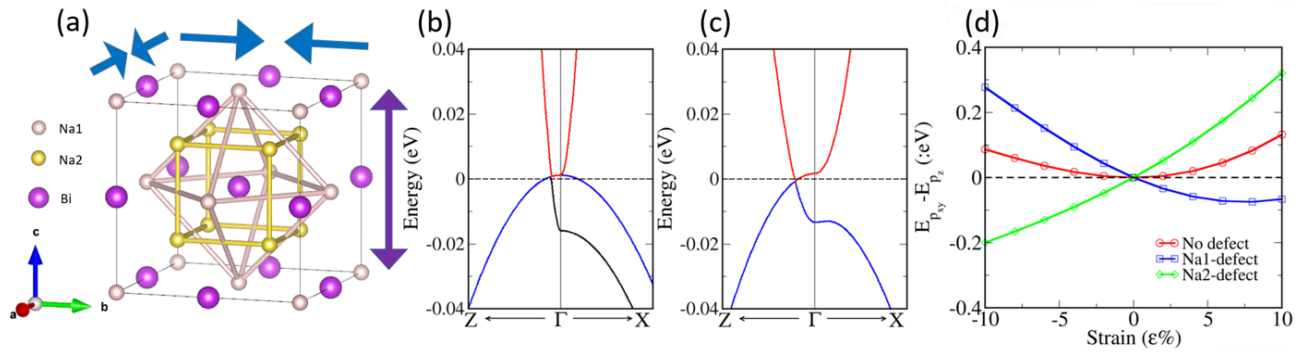

FIG. 6. (a)schematic diagram of the Fm$\bar{3}$m phase with uniaxial strain. Six Na1 atoms (pink) next-nearest neighbour around the body-centered Bi (purple) form an octahedron while eight Na2 (yellow) nearest neighbour around form a cubic; (b) and (c) The band structures near Γ point of Na_3Bi in the space group of $I4/mmm$ which comes from uniaxial strain along z axis on the Fm$\bar{3}$m phase without and with spin orbital coupling. The red and blue lines correspond to CBM and VBM respectively. (d) The energy difference between $|Bi, p_{x,y}>$ and $|Bi, p_z>$ near the fermi level vs. uniaxial strains in the range of $-10\% \leq \epsilon \leq 10\%$ for the intact, Na1-absent and Na2-absent Na_3Bi.

TABLE V. The product of the parities for all the occupied bands at eight TRIMs for the Fm$\bar{3}$m phase of Na_3Bi with shear strain along ⟨100⟩ axis.

TRIM	Γ	2S	2R	2T	X ;	total
Parity	−	−	−	+	+ ;	−

B. SHEAR STRAIN ALONG the ⟨100⟩ DIRECTION ON the Fm$\bar{3}$m PHASE

Shear strain might have different effect on the electronic structures compared with tensile or compressive strain. If we impose a shear strain along ⟨100⟩ direction on the original Fm$\bar{3}$m structure, we will get a structure in the space group of I/mmm which belongs to the D_{2h} point group. In fact, as shown in Fig. 7 (a), this operation only slightly changes one of the three lattice angles. The green line in Fig. 4 (b) shows how shear strain energy $E_{ss\langle 001\rangle}$ varies with the angle parameter γ ranging from 85° to 95°. It seems that the shear stain costs a large mount of energy. Here we take the change of γ from 90°to 86°as an example. Electronic band structure shown in Fig. 7(b) indicates that the resulting structure is an insulator with a small gap of around 17 meV. The D_{2h} point group ensures the existence of the inversion symmetry in the shear-strained structure, which enables us to calculate Z_2 by multiplying the parities for all the occupied Bloch states at the eight TRIMs using Fu and Kane's method[60]. The results are listed in Table. V, which clearly show $Z_2 = 1$. Thus shear strain along the ⟨100⟩ direction brings the system from a semimetal into a TI.

In fact, the shear strain changes the point group from O_h to D_{2h}, which also affects the $\mathbf{k}\cdot\mathbf{p}$ Hamiltonian dramatically. After a careful analysis of the symmetry and a tedious derivation, one can give the character table of the Γ matrice and the polynomials of momentum $\vec{k}$ as shown in Table. VI.

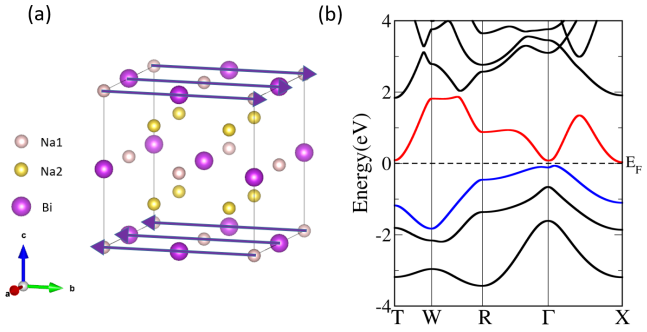

FIG. 7. (a)Crystal structure of Fm$\bar{3}$m Na_3Bi under ⟨100⟩ shear strain. The purple arrows represent shear strains on the top and bottom surfaces. (b)Corresponding band structures (with SOC) of Na_3Bi under the ⟨100⟩ shear strain. The red and blue lines correspond to CBM and VBM, respectively.

TABLE VI. The character table for the Fm$\bar{3}$m phase of Na_3Bi with shear strain along ⟨100⟩ axis.

Γ	Representation	T	$\vec{k}$
$\Gamma_0 = I$	$\tilde{\Gamma}_1^+$	+	$1, k_x^2, k_y^2, k_z^2$
Γ_1	$\tilde{\Gamma}_3^+$	+	$k_y k_z$
Γ_2	$\tilde{\Gamma}_2^+$	+	$k_z k_x$
Γ_3	$\tilde{\Gamma}_4^+$	+	$k_x k_y$
Γ_4	$\tilde{\Gamma}_1^+$	+	$1, k_x^2, k_y^2, k_z^2$
Γ_5	$\tilde{\Gamma}_1^+$	+	$1, k_x^2, k_y^2, k_z^2$

Finally, from Table. VI, our model Hamiltonian yields

$$\begin{aligned} H &= \sum_{i=0}^{5} f_i(\vec{k})\Gamma_i \\ &= \sum_{i=0,4,5} (a_i + b_{ix}k_x^2 + b_{iy}k_y^2 + b_{iz}k_z^2)\Gamma_i \\ &+ c_1 k_y k_z \Gamma_1 + c_2 k_z k_x \Gamma_2 + c_3 k_x k_y \Gamma_3. \end{aligned} \tag{5}$$

It's clear that the band gap in the sheared structure comes from $a_4\Gamma_4 + a_5\Gamma_5$, which depends on the point group D_{2h} completely. Similarly, a band crossing of above-mentioned model requires $f_1 = f_2 = f_3 = f_4 = f_5 = 0$, i.e. $k_\alpha = k_\beta = 0 \cap k_\gamma \neq 0 \cap \frac{a_{4\gamma}}{b_{4\gamma}} = \frac{a_{5\gamma}}{b_{5\gamma}} < 0$. Here α, β, γ is a permutation of $\{x, y, z\}$. It means that we can find a Dirac crossing along k_γ direction only when $\frac{a_{4\gamma}}{b_{4\gamma}} = \frac{a_{5\gamma}}{b_{5\gamma}} < 0$ stands, and the location of the crossing is $k_\alpha = k_\beta = 0, k_\gamma = \pm\sqrt{-\frac{a_{5\gamma}}{b_{5\gamma}}}$. However, from our ab initio calculations, a gap always exists when shear deformation along the $\langle 100\rangle$ axis (γ) is in the range of $85-95°$. In fact, $\frac{a_{4\gamma}}{b_{4\gamma}} = \frac{a_{5\gamma}}{b_{5\gamma}} < 0$ is a very rigorous condition, which can not be obtained without imposing other symmetries. Thus a gap near Γ will always occur. On the other hand, the Z_2 invariant remains unchanged because of the same reason discussed for the uniaxial-strained case. Therefore, the splitting of crystal field together with SOC generates $a_4\Gamma_4$ and $a_5\Gamma_5$ in the Hamiltonian, and results in the topological nontrivial band gap at Γ point.

C. SHEAR STRAIN ALONG the $\langle 111\rangle$ DIRECTION ON the Fm$\bar{3}$m PHASE

Then we consider the case of shear strain along the body diagonal direction as Fig. 8(a) shows. This type of strain turns the space group of the structure from Fm$\bar{3}$m to R$\bar{3}$m (belongs to the D_{3d} point group). In fact, this type of strain can also be obtained by changing the α, β and γ by the same amplitude, which can be seen as a combination of shear strains along the $\langle 100\rangle$ $\langle 010\rangle$,$\langle 001\rangle$ directions. The red line in Fig. 4 (b) shows how shear strain energy $E_{ss\langle 111\rangle}$ varies with the angle parameter $\alpha = \beta = \gamma$ ranging from 85° to 95°. Here we choose $\alpha = \beta = \gamma = 92°$as an example.

The corresponding band structure shown in Fig. 8(b) indicates an insulator phase. Due to the preservation of IS, we calculate the product of the parities for the occupied bands at all the eight TRIMs, the result is shown in Table. VII. Parity inversion at the Γ point leads to a nontrivial band topology with $Z_2 = (1, 000)$, which indicates that this $\langle 111\rangle$ sheared structure is a strong TI.

After similar analysis of the symmetry and derivation, we can give the character table of Γ matrices and the polynomials of momentum $\vec{k}$ for the case of $\langle 111\rangle$ shear strain as Table. VIII shows. As a result, we can obtain

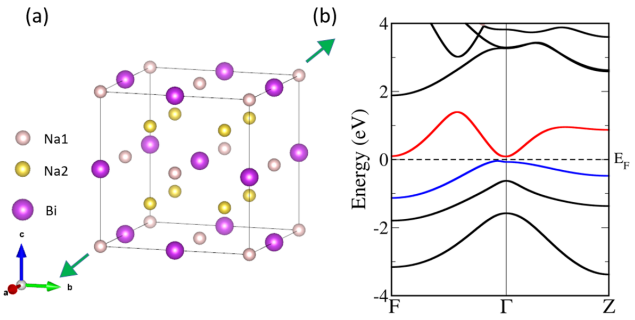

FIG. 8. (a)Crystal structure of Na_3Bi with Fm$\bar{3}$m symmetry under shear strain in $\langle 111\rangle$ direction. The green arrows represents the shear direction. (b)Corresponding band structure (with SOC) of Na_3Bi with the $\langle 111\rangle$ shear strain. The red and blue lines correspond to CBM and VBM respectively.

TABLE VII. The product of the parities for all the occupied bands at the eight TRIMs for the Fm$\bar{3}$m phase of Na_3Bi with shear strain along the $\langle 111\rangle$ axis.

TRIM	Γ	3L	3FB	T ;	total
Parity	−	+	+	+ ;	−

the corresponding $\mathbf{k}\cdot\mathbf{p}$ Hamiltonian as

$$\begin{aligned} H &= \sum_{i=0}^{5} f_i(\vec{k})\Gamma_i \\ &= [a_0 + b_0(k_x^2 + k_y^2) + c_0 k_z^2]\Gamma_0 + a_{12}(k_y k_z \Gamma_1 + k_x k_z \Gamma_2) \\ &+ b_{12}[(-2k_x k_y)\Gamma_1 + (k_x^2 - k_y^2)\Gamma_2] \\ &+ a_{34}[2k_x k_y \Gamma_3 + (k_x^2 - k_y^2)\Gamma_4] \\ &+ b_{34}[k_y k_z \Gamma_3 - k_x k_z \Gamma_4] \\ &+ [a_5 + b_5(k_x^2 + k_y^2) + c_5 k_z^2]\Gamma_5. \end{aligned} \tag{6}$$

Similarly, a band crossing of this model requires $f_1 = f_2 = f_3 = f_4 = f_5 = 0$. It can be classified into two cases. (a)$k_x = k_y = 0 \cap k_z \neq 0 \cap a_5 c_5 < 0$, (b)$\frac{a_{12}}{b_{12}} = -\frac{b_{34}}{a_{34}} \cap k_z \neq 0 \cap (a_5 b_5 < 0 \cup a_5 c_5 < 0)$. In the case of (b), if $\frac{-a_5 a_{12}^2}{b_5 a_{12}^2 + c_5 b_{12}^2} > 0$, we can define $l = \sqrt{\frac{-a_5 a_{12}^2}{b_5 a_{12}^2 + c_5 b_{12}^2}}$, then six Dirac points locating at $(\mp l, 0, \pm\frac{b_{12}}{a_{12}} l)$, $(\pm\frac{1}{2} l, \pm\frac{\sqrt{3}}{2} l, \pm\frac{b_{12}}{a_{12}} l)$ and $(\pm\frac{1}{2} l, \mp\frac{\sqrt{3}}{2} l, \pm\frac{b_{12}}{a_{12}} l)$ can be found. It's obvious that they are related to each other by R_{3z} symmetries. However, it should be noted that the condition of $\frac{a_{12}}{b_{12}} = -\frac{b_{34}}{a_{34}}$ in case (b) is very rigorous and can not be obtained without other symmetries, i.e., case (a) is a unique condition for a stable DSM. Thus, as discussed in the case of uniaxial strain, this system belongs to TI when $a_5 c_5 > 0$, while it transforms into a DSM only in the case of $a_5 c_5 < 0$. As a

TABLE VIII. The character table for the Fm$\bar{3}$m phase of Na_3Bi with shear strain along the $\langle 111 \rangle$ axis.

Γ	Representation	T	$\vec{k}$
$\Gamma_0 = I$	$\tilde{\Gamma}_1^+$	+	$1, k_x^2+k_y^2+k_z^2$
$\{\Gamma_1, \Gamma_2\}$	$\tilde{\Gamma}_3^+$	+	$\{k_yk_z, k_xk_z\}; \{-2k_xk_y, k_x^2-k_y^2\}$
$\{\Gamma_3, \Gamma_4\}$	$\tilde{\Gamma}_3^+$	+	$\{2k_xk_y, k_x^2-k_y^2\}; \{k_yk_z, -k_xk_z\}$
Γ_5	$\tilde{\Gamma}_1^+$	+	$1, k_x^2+k_y^2+k_z^2$

result, this system have the same phase diagram as shown in Fig. 5. Similar to the shear strain along $\langle 100 \rangle$ direction case, from our ab initio calculations, a gap always exists when shear deformation along the the $\langle 111 \rangle$ axis ($\alpha = \beta = \gamma$) is in the range of $85 - 95°$. Which indicates that $a_5c_5 > 0$ always stands for this shear strain. Due to the similar reason as discussed in the case of uniaxial strain, the gap induced by $a_5\Gamma_5$ term from D_{3d} symmetry will always remain and the Z_2 will not change.

VI. SURFACE STATES OF THE FM$\bar{3}$M PHASE WITHOUT AND WITH STRAIN

Exotic topological surface states is an important property to identify various topological phases. Based on the tight-binding model constructed with MLWFs (maximally localised Wannier functions) method[61–63], we have calculated the projected surface states of the Fm$\bar{3}$m Na_3Bi without strain and with different type of strains, as shown in Fig. 9. As showed in Fig. 9(a), there is no topological protected surface states in the Fm$\bar{3}$m Na_3Bi without strain. When we impose a uniaxial strain on Fm$\bar{3}$m Na_3Bi, a Dirac crossing appears near the Γ point in the bulk band structure. And the corresponding non-trivial surface states connecting the Dirac point also emerges, as showed in Fig. 9(b). As dicusssed above and showed in Fig. 9(c) and Fig. 9(d), shear strains along the $\langle 100 \rangle$ and $\langle 111 \rangle$ directions induce the original system into TIs, nontrivial metallic surface states can be found in the gap.

VII. CONCLUSION

In conclusion, with first-principle calculations we investigate the effect of stress/strain on Na_3Bi, a native 3D Dirac semimetal, and find strains have large effects on the topological band structures of this system. We apply a uniaxial strain to break the R_{3z} symmetry on the ambient P$\bar{3}$c1 phase and find that this strain tunes Na_3Bi into a TI with a topological nontrivial gap at Γ point. Ab initio calculations show that the high pressure Fm$\bar{3}$m phase is a new type of semimetal with the unique parabolic touching point at Γ point on the Fermi level, which can be well described by a Luttinger Hamiltonian. According to our calculations, uniaxial strain along the $\langle 001 \rangle$ direction can tune the high pressure Fm$\bar{3}$m Na_3Bi from the parabolic semimetal into a DSM, while shear strain along both the $\langle 100 \rangle$ and $\langle 111 \rangle$ directions can tune the high pressure Fm$\bar{3}$m phase from the parabolic semimetal into a TI. To gain more insights on these quantum phase transition from strain, we derive three $\mathbf{k}\cdot\mathbf{p}$ models for the Fm$\bar{3}$m phase and with all kinds of shear strains. It is obvious that SOC together with the splitting of crystal field from strains we imposed play key roles for the topological phase transitions in Na_3Bi. In the end, we calculated surface states of Fm$\bar{3}$m Na_3Bi without strain and with different types of strains to verify these topological transitions. Different substrate might be used to introduce strain on samples grew on them, which might be used to examine the topological phase transitions studied in this work.

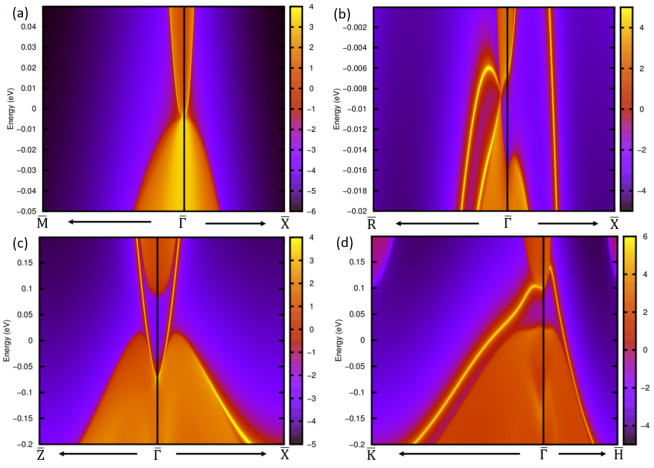

FIG. 9. The projected surface states of Fm$\bar{3}$m Na_3Bi (a)without strain and terminated in $\langle 100 \rangle$ direction; (b)under uniaxial strain and terminated in $\langle 100 \rangle$ direction; (c)under shear strain in $\langle 001 \rangle$ direction and terminated in $\langle 100 \rangle$ direction; (d)under shear strain in $\langle 111 \rangle$ direction and terminated in $\langle 100 \rangle$ direction respectively.

VIII. ACKNOWLEDGMENTS

We thank the fruitful discussions with Huaiqiang Wang, Mengnan Chen, Feng Tang and Yongping Du. This work is supported by the MOST of China (Grant Nos: 2016YFA0300404, 2015CB921202), the National Natural Science Foundation of China (Grant Nos: 51372112, 11574133 and 13001049), NSF Jiangsu province (No. BK20150012), the Fundamental Research Funds for the Central Universities (No. 020414380068/1-1), Special Program for Applied Research on Super Computation of the NSFC-Guangdong Joint Fund (the second phase), and Open Fund of Key Laboratory for Intelligent Nano Materials and Devices of the Ministry of Education (INMD-2016M01). Part of the calculations were performed on the supercomputer in the HPCC of Nanjing University and "Tianhe-2" at NSCC-Guangzhou.

* To whom correspondence should be addressed. E-mail: jiansun@nju.edu.cn

[1] M. Z. Hasan and C. L. Kane, Rev. Mod. Phys. **82**, 3045 (2010).

[2] X.-L. Qi and S.-C. Zhang, Rev. Mod. Phys. **83**, 1057 (2011).

[3] A. A. Burkov, M. D. Hook, and L. Balents, Phys. Rev. B **84**, 235126 (2011).

[4] H. Weng, X. Dai, and Z. Fang, J. Phys.: Conden. Matter **28**, 303001 (2016).

[5] O. Pankratov, S. Pakhomov, and B. Volkov, Solid State Commun. **61**, 93 (1987).

[6] B. A. Bernevig, T. L. Hughes, and S.-C. Zhang, Science **314**, 1757 (2006).

[7] D. Hsieh, Y. Xia, D. Qian, L. Wray, J. H. Dil, F. Meier, J. Osterwalder, L. Patthey, J. G. Checkelsky, and N. P. Ong, Nature **460**, 1101 (2009).

[8] H. Zhang, C. X. Liu, X. L. Qi, X. Dai, Z. Fang, and S. C. Zhang, Nat. Phys. **5**, 438 (2009).

[9] Z. Wang, Y. Sun, X.-Q. Chen, C. Franchini, G. Xu, H. Weng, X. Dai, and Z. Fang, Phys. Rev. B **85**, 195320 (2012).

[10] Z. Wang, H. Weng, Q. Wu, X. Dai, and Z. Fang, Phys. Rev. B **88**, 125427 (2013).

[11] X. Wan, A. M. Turner, A. Vishwanath, and S. Y. Savrasov, Phys. Rev. B **83**, 205101 (2011).

[12] G. Xu, H. Weng, Z. Wang, X. Dai, and Z. Fang, Phys. Rev. Lett. **107**, 186806 (2011).

[13] B. Q. Lv, H. M. Weng, B. B. Fu, X. P. Wang, H. Miao, J. Ma, P. Richard, X. C. Huang, L. X. Zhao, G. F. Chen, Z. Fang, X. Dai, T. Qian, and H. Ding, Phys. Rev. X **5**, 031013 (2015).

[14] S. Y. Xu, I. Belopolski, N. Alidoust, M. Neupane, G. Bian, C. Zhang, R. Sankar, G. Chang, Z. Yuan, and C. C. Lee, Science **349**, 613 (2015).

[15] H. Weng, Y. Liang, Q. Xu, R. Yu, Z. Fang, X. Dai, and Y. Kawazoe, Phys. Rev. B **92**, 045108 (2015).

[16] R. Yu, H. Weng, Z. Fang, X. Dai, and X. Hu, Phys. Rev. Lett. **115**, 036807 (2015).

[17] Y. Kim, B. J. Wieder, C. L. Kane, and A. M. Rappe, Phys. Rev. Lett. **115**, 036806 (2015).

[18] G. Bian, T.-R. Chang, R. Sankar, S.-Y. Xu, H. Zheng, T. Neupert, C.-K. Chiu, S.-M. Huang, G. Chang, I. Belopolski, D. S. Sanchez, M. Neupane, N. Alidoust, C. Liu, B. Wang, C.-C. Lee, H.-T. Jeng, C. Zhang, Z. Yuan, S. Jia, A. Bansil, F. Chou, H. Lin, and M. Z. Hasan, Nat. Commun. **7**, 10556 (2016).

[19] T. Bzdusek, Q. Wu, A. Ruegg, M. Sigrist, and A. A. Soluyanov, Nature **538**, 75 (2016).

[20] R. Li, H. Ma, X. Cheng, S. Wang, D. Li, Z. Zhang, Y. Li, and X.-Q. Chen, Phys. Rev. Lett. **117**, 096401 (2016).

[21] K. S. Novoselov, A. K. Geim, S. V. Morozov, D. Jiang, M. I. Katsnelson, I. V. Grigorieva, S. V. Dubonos, and A. A. Firsov, Nature **438**, 197 (2005).

[22] A. K. Geim and K. S. Novoselov, Nat. Mater. **6**, 183 (2007).

[23] S. M. Young, S. Zaheer, J. C. Y. Teo, C. L. Kane, E. J. Mele, and A. M. Rappe, Phys. Rev. Lett. **108**, 140405 (2012).

[24] Q. D. Gibson, L. M. Schoop, L. Muechler, L. S. Xie, M. Hirschberger, N. P. Ong, R. Car, and R. J. Cava, Phys. Rev. B **91**, 205128 (2015).

[25] M. Z. Hasan and J. E. Moore, Ann. Rev. Condens. Matter Phys. **2**, 55 (2011).

[26] Z. K. Liu, J. Jiang, B. Zhou, Z. J. Wang, Y. Zhang, H. M. Weng, D. Prabhakaran, S. K. Mo, H. Peng, and P. Dudin, Nat. Mater. **13**, 677 (2014).

[27] M. Neupane, S.-Y. Xu, R. Sankar, N. Alidoust, G. Bian, C. Liu, I. Belopolski, T.-R. Chang, H.-T. Jeng, H. Lin, A. Bansil, F. Chou, and M. Z. Hasan, Nat. Commun. **5** (2014).

[28] S. Borisenko, Q. Gibson, D. Evtushinsky, V. Zabolotnyy, B. Büchner, and R. J. Cava, Phys. Rev. Lett. **113**, 027603 (2014).

[29] H. Yi, Z. Wang, C. Chen, Y. Shi, Y. Feng, A. Liang, Z. Xie, S. He, J. He, and Y. Peng, Sci. Rep. **4**, 6106 (2013).

[30] S. Jeon, B. B. Zhou, A. Gyenis, B. E. Feldman, I. Kimchi, A. C. Potter, Q. D. Gibson, R. J. Cava, A. Vishwanath, and A. Yazdani, Nat. Mater. **13**, 851 (2014).

[31] Y. L. Chen, Z. K. Liu, B. Zhou, Y. Zhang, Z. J. Wang, H. M. Weng, D. Prabhakran, S. K. Mo, Z. X. Shen, and Z. Fang, Science **343**, 864 (2014).

[32] S. Y. Xu, C. Liu, S. K. Kushwaha, R. Sankar, J. W. Krizan, I. Belopolski, M. Neupane, G. Bian, N. Alidoust, and T. R. Chang, Science **347**, 294 (2015).

[33] A. C. Potter, I. Kimchi, and A. Vishwanath, Nat. Commun. **5**, 5161 (2014).

[34] J. Xiong, S. K. Kushwaha, T. Liang, J. W. Krizan, M. Hirschberger, W. Wang, R. J. Cava, and N. P. Ong, Science **350**, 413 (2015).

[35] P. Goswami, J. H. Pixley, and S. Das Sarma, Phys. Rev. B **92**, 075205 (2015).

[36] S. A. Kulinich, M. E. Leonova, and L. G. Sevast'Yanova, Zh. Obshch. Khim. **69**, 681 (1999).

[37] X. Cheng, R. Li, Y. Sun, X.-Q. Chen, D. Li, and Y. Li, Phys. Rev. B **89**, 245201 (2014).

[38] F. Guinea, M. I. Katsnelson, and A. K. Geim, Nat. Phys. **6**, 30 (2009).

[39] M. Bahramy, B.-J. Yang, R. Arita, and N. Nagaosa, Nat. Commun. **3**, 679 (2012).

[40] J. Ruan, S.-K. Jian, H. Yao, H. Zhang, S.-C. Zhang, and D. Xing, Nat. Commun. **7**, 11136 (2016).

[41] S. Zhang, Q. Wu, L. Schoop, M. N. Ali, Y. Shi, N. Ni, Q. Gibson, S. Jiang, V. Sidorov, W. Yi, J. Guo, Y. Zhou, D. Wu, P. Gao, D. Gu, C. Zhang, S. Jiang, K. Yang, A. Li, Y. Li, X. Li, J. Liu, X. Dai, Z. Fang, R. J. Cava, L. Sun, and Z. Zhao, Phys. Rev. B **91**, 165133 (2015).

[42] L. He, Y. Jia, S. Zhang, X. Hong, C. Jin, and S. Li, npj Quantum. Mater. **1**, 16014 (2016).

[43] H. Wang, H. Wang, H. Liu, H. Lu, W. Yang, S. Jia, X.-J. Liu, X. Xie, J. Wei, and J. Wang, Nat. mater. **15**, 38 (2016).

[44] Y. Zhou, P. Lu, Y. Du, X. Zhu, G. Zhang, R. Zhang, D. Shao, X. Chen, X. Wang, M. Tian, J. Sun, X. Wan, Z. Yang, W. Yang, Y. Zhang, and D. Xing, Phys. Rev. Lett. **117**, 146402 (2016).

[45] Y. Zhou, J. Wu, W. Ning, N. Li, Y. Du, X. Chen, R. Zhang, Z. Chi, X. Wang, X. Zhu, P. Lu, C. Ji, X. Wan, Z. Yang, J. Sun, W. Yang, M. Tian, Y. Zhang, and H.-k. Mao, Proc. Natl. Acad. of Sci. USA **113**, 2904 (2016).

[46] P. Lu, J.-S. Kim, J. Yang, H. Gao, J. Wu, D. Shao, B. Li, D. Zhou, J. Sun, D. Akinwande, D. Xing, and J.-F. Lin, Phys. Rev. B **94**, 224512 (2016).

[47] X. Chen, P. Lu, X. Wang, Y. Zhou, C. An, Y. Zhou, C. Xian, H. Gao, Z. Guo, C. Park, B. Hou, K. Peng, X. Zhou, Y. Xiong, J. Sun, Z. Yang, D. Xing, and Y. Zhang, ArXiv e-prints (2016), arXiv:1608.06763.
[48] Y. Li, Y. Zhou, Z. Guo, X. Chen, P. Lu, X. Wang, C. An, Y. Zhou, J. Xing, G. Du, X. Zhu, H. Yang, J. Sun, Z. Yang, Y. Zhang, and H.-H. Wen, arXiv preprint arXiv:1611.02548 (2016).
[49] X. Cheng, R. Li, D. Li, Y. Li, and X.-Q. Chen, Phys. Chem. Chem. Phys. **17**, 6933 (2015).
[50] X. Cheng, R. Li, D. Li, Y. Li, and X.-Q. Chen, Phys. Rev. B **92**, 155109 (2015).
[51] M. E. Leonova, S. A. Kulinich, and L. G. Sevast'syanova, Exp. Geosci. **7**, 55 (1998).
[52] M. E. Leonova, I. K. Bdikin, S. A. Kulinich, O. K. Gulish, L. G. Sevast'Yanova, and K. P. Burdina, Inorg. Mater. **39**, 266 (2003).
[53] J. M. Luttinger, Phys. Rev. **102**, 1030 (1956).
[54] C. J. Pickard and R. J. Needs, Phys. Rev. Lett. **97**, 045504 (2006).
[55] C. J. Pickard and R. J. Needs, J. Phys.: Conden. Matter **23**, 053201 (2011).
[56] G. Kresse and D. Joubert, Phys. Rev. B **59**, 1758 (1999).
[57] J. P. Perdew, K. Burke, and M. Ernzerhof, Phys. Rev. Lett. **77**, 3865 (1996).
[58] G. Kresse and J. Furthmüller, Phys. Rev. B **54**, 11169 (1996).
[59] P. Blaha, K. Schwarz, G. Madsen, D. Kvasnicka, and J. Luitz, *WIEN2k: An Augmented Plane Wave plus Local Orbitals Program for Calculating Crystal Properties* (Karlheinz Schwarz, Technische Universitaet Wien, Vienna, 2001).
[60] L. Fu and C. L. Kane, Phys. Rev. B **76**, 045302 (2007).
[61] N. Marzari and D. Vanderbilt, Phys. Rev. B **56**, 12847 (1997).
[62] I. Souza, N. Marzari, and D. Vanderbilt, Phys. Rev. B **65**, 035109 (2001).
[63] N. Marzari, A. A. Mostofi, J. R. Yates, I. Souza, and D. Vanderbilt, Rev. Mod. Phys. **84**, 1419 (2012).